Colloids and Surfaces B: Biointerfaces 212 (2022) 112346

Contents lists available at ScienceDirect

Colloids and Surfaces B: Biointerfaces

journal homepage: www.elsevier.com/locate/colsurfb

Electronic properties and surface potential evaluations at the protein nano-biofilm/oxide interface: Impact on corrosion and biodegradation

Ehsan Rahimi [a,*,1], Ruben Offoiach [a], Maria Lekka [b,*,2], Lorenzo Fedrizzi [a]

[a] Polytechnic Department of Engineering and Architecture, University of Udine, 33100 Udine, Italy
[b] CIDETEC, Basque Research and Technology Alliance (BRTA), Po. Miramón 196, 20014 DonostiaSan Sebastián, Spain

ARTICLE INFO

Keywords:
Albumin protein adsorption
SKPFM
Protein surface potential
Space charge capacitance
Corrosion

ABSTRACT

The formation of a protein nano-biofilm, which exhibits a special electronic behavior, on the surface of metals or oxide biomaterials considerably influences the crucial subsequent interactions, particularly the corrosion and biodegradation processes. This study discusses the impact of electrical surface potential (ESP) of a single or nano-biofilm of albumin protein on the electrochemical interactions and electronic property evolutions (e.g., charge carriers, space charge capacitance (SCC), and band bending) occurring on the surface oxide of CoCrMo implants. Scanning Kelvin probe force microscopy (SKPFM) results indicated that ESP or surface charge distribution on a single or nano-biofilm of the albumin protein is lower than that of a CoCrMo complex oxide layer, which hinders the charge transfer at the protein/electrolyte interface. Using a complementary approach, which involved performing Mott-Schottky analysis at the electrolyte/protein/oxide interface, it was revealed that the albumin protein significantly increases the SCC magnitude and number of n-type charge carrier owing to increased band bending at the SCC/protein interface; this facilitated the acceleration of metal ion release and metal-protein complex formation. The nanoscale SKPFM and electrochemical analyses performed in this study provide a better understanding of the role of protein molecules in corrosion/biodegradation of metallic biomaterials at the protein nano-biofilm/oxide interface.

1. Introduction

Protein adsorption on solid surfaces (such as metallic, ceramic, and polymer surfaces) is an initial quick stage (millisecond-second scale) whereby medical biomaterials are incorporated into the human physiological media [1]. The amount and type of adsorbed protein, as well as its conformational arrangement, control some crucial interactions subsequent to the formation of the protein nano-biofilm, including the adhesion and proliferation of the cell, inflammatory responses, and particularly the metal ion release process [2,3]. Protein adsorption on implanted biomaterial surfaces involves complex interactions, including hydrophobic, electrostatic, van der Waals, and hydrogen bonding [4]. In addition, the charge, concentration, and hydrophobicity of the protein, along with the pH, ionic strength, and agitation of the electrolyte, considerably control the adsorption mechanism of the protein molecule [1,5].

Proteins are electrically conductive materials possessing distinct electrical conductivities (ECs); EC strongly depends on the amino acid composition and molecular structure of the proteins [6], and can influence the electrochemical interactions and metal ion release at the protein nano bio-film/homogeneous or heterogeneous oxide interface [7–9]. A wide range of experimental techniques under in situ (in the electrolyte) and ex situ (in air or vacuum) conditions have been employed to study the EC of biological molecules, particularly proteins. These experimental approaches provide in-depth knowledge of the EC of the adsorbed proteins on solid surfaces, including cyclic voltammetry [10,11], sandwiching proteins between two solid electrodes [12,13], scanning tunneling microscopy (STM) [14–16], conductance atomic force microscopy (C-AFM) [17,18], and scanning Kelvin probe force microscopy (SKPFM) [7,18,19]. A study by Ron et al. showed that the high EC of azurin and bacteriorhodopsin protein molecules is related to tryptophan residues in their chemical structure [6,20]. In addition, using C-AFM, Xu et al. reported that the higher conductivity of holoferritin than apoferritin protein is due to a highly conductive core in the

* Corresponding authors.
E-mail addresses: rahimi.ehsan@spes.uniud.it (E. Rahimi), mlekka@cidetec.es (M. Lekka).
[1] orcid-id: 0000-0002-7128-8940.
[2] orcid-id: 0000-0001-6811-3843.

https://doi.org/10.1016/j.colsurfb.2022.112346
Received 16 November 2021; Received in revised form 15 January 2022; Accepted 17 January 2022
Available online 20 January 2022

central molecular structure of holoferritin, which is more conductive than the shell [21]. In contrast, the EC results of serum albumin protein from solid-state measurements indicated that albumin protein has a lower EC than other proteins, which can hinder electrochemical interaction at the electrolyte/protein/solid interface via adsorption on the metal and oxide surfaces [6,12].

Among the various approaches reported for the EC of biological soft matter, SKPFM is undeniably a very surface sensitive technique [22,23] that can be used to measure the local electrical potential or surface charge distribution in different simple or complex systems, including microelectronics [24,25], organic [22,26] and inorganic thin films [27], and biological species (for e.g., proteins [28] and DNA [29,30]), with a high spatial resolution. Therefore, at high lateral and electrical resolutions, crucial information can be obtained regarding the charging and discharging processes in a single molecule [27] or localized charge distribution on DNA [31] and proteins [32]. This significant surface sensitivity of SKPFM to any type of chemical variation, structural change, or surface defect enables the prediction of electrochemical interactions at the protein nano-biofilm/solid surface interface [18,19,33]. For example, in our previous research, we investigated the capability of SKPFM to visualize the hindering effect of hydrogen peroxide on the dense film formation of albumin protein regions on titanium-based alloy surfaces in phosphate buffered saline (PBS) solution.

For many years, Co-based alloys, particularly cobalt-chromium-molybdenum (CoCrMo), have been extensively considered as biocompatible metallic biomaterials for orthopedic implants such as hip and knee joint replacements [34–37]. These alloys are favored in biomedical applications owing to their overall high wear resistance and good biocompatibility, which are linked to superior corrosion resistance, and is mainly generated by the spontaneous formation of a compact and thin passive film (1–4 nm) on the alloy surface [38]. Based on prior surface analysis reports, the chemical composition of the CoCrMo passive film mainly includes Cr_2O_3 with a lower distribution of Co and Mo oxides [39,40]. However, in human physiological media, which is a complex and aggressive environment with various ions, proteins, and cells, the protective passive film on the CoCrMo surface is susceptible to surface degradation; in turn, the CoCrMo alloy loses biocompatibility, eventually leading to implant failure [41–43]. The corrosion or metal ion release process of all metallic implants in human physiological media causes toxic and allergenic reactions, inflammation, and cancer expansion [44]. Some critical properties of the formed oxide layer, including the roughness, chemical composition, electronic properties, surface charge, and defects, significantly influence the protein film formation, particularly affecting the electrochemical interactions at the protein nano-biofilm/oxide surface interface [45].

An oxide film with semiconductor characteristics (donor or acceptor charge carriers), during contact with a solid surface (metals and semiconductor oxides) or electrolyte media, can induce a space charge region (SCR) at the contact interface owing to the difference in their Fermi energy levels (E_f), resulting in bending of the valence and conduction bands (E_v and E_c) at the surface of the semiconductor oxide [46,47]. It has been well established that some phenomena, including the applied potential [48], pH [49], temperature [50], and organic and inorganic species (calcium, phosphate, hydrogen peroxide)[51] in electrolytes, considerably affect the magnitude of band bending and the capacitance of the SCR. In particular, the presence of a thin film of adsorbed proteins such as human or bovine serum albumin (HSA and BSA) on the semiconductor oxide surface can remarkably modify the charge carrier density and flat band potential (E_{ft}) distribution within the oxide layer [52].

In addition, an adsorbed organic layer of proteins and/or cells on metallic surfaces is accompanied by some simultaneous or consecutive events, including decreased participation of the calcium/phosphate species, cathodic reactions [51,53,54], and reduced diffusion of the ions and molecules (as a barrier layer) [1]. Indeed, the chemical composition and electronic property (e.g., the EC and/or electron transfer properties) in the protein molecule structures are the determining step in electrochemical redox reactions and also affect the charge carrier distribution at the protein nano-biofilm/oxide layer interface [12,19,55,56]. However, as an electronic property at the adsorbed protein/oxide layer interface, direct evidence of the electrical surface potential evaluations and its effect on the semiconductor characteristics (donor or acceptor carriers), and in turn the biodegradation mechanism, has not been established. In this study, using combined AFM/SKPFM and Mott-Schottky (MS) analysis, we elucidate the following: (1) the adsorption morphology and electrical surface potential evolution of the BSA protein with various concentrations 0, 0.5, and 2 $g{\cdot}L^{-1}$ during adsorption on the CoCrMo oxide surface; (2) the electrical surface potential of a single BSA protein and its effect on the energy band diagrams; (3) the impact of the applied anodic potentials including + 100 mV and + 300 mV vs. Ag/AgCl on the distribution of semiconductor characteristics in the SCR of the oxide layer in the BSA protein media; and (4) the effect of protein molecules on the charge carriers, flat band potential, and corrosion/biodegradation mechanisms at the BSA nano-biofilm/oxide layer interface.

2. Experimental procedure

2.1. Sample and electrolyte preparations

The specimens were cut from the bulk CoCrMo (ASTM F1537) alloy in the form of cuboids with a surface area of approximately 1 cm^2 and thickness of 5 mm. The chemical composition (wt%) of the CoCrMo alloy was 0.05 C, 0.39 Si, 0.45 Mn, 0.004 P, 0.001 S, 27.77 Cr, 5.08 Mo, 0.25 Ni, 0.005 Ti, 0.38 Fe, and 0.22 N (Co balance). The specimens were wet ground from #500 to #4000 meshes with SiC abrasive foil and then polished with alumina slurry to achieve a mirror-like surface. Finally, the samples were cleaned in an acetone ultrasonic bath for 30 min, washed with deionized water, and finally dried by air blowing. PBS solution was prepared according to the ASTM Standard (F2129) [57], and the chemical composition was 8 $g{\cdot}L^{-1}$ NaCl, 0.2 $g{\cdot}L^{-1}$ KCl, 1.15 $g{\cdot}L^{-1}$ Na_2HPO_4, and 0.2 $g{\cdot}L^{-1}$ KH_2PO_4. Protein media with two different concentrations including 0.5 and 2 $g{\cdot}L^{-1}$ BSA was prepared by adding lyophilized BSA powder (Sigma–Aldrich, ≥96% agarose gel electrophoresis) to the PBS solution. The pH values of all solutions were controlled by a pH meter (GLP 21, CRISON), close to 7.4 ± 1 at 37 °C for all the electrochemical measurements.

2.2. Microstructure characterization and scanning probe microscope (SPM) measurements

To investigate the BSA adsorption morphology, electrical surface potential, and its effect on the surface potential distribution on the CoCrMo complex oxide film, AFM and SKPFM measurements were performed. AFM and SKPFM maps were obtained for the CoCrMo specimens after 1 h immersion in the PBS solution containing 0, 0.5, and 2 $g{\cdot}L^{-1}$ BSA concentrations (static and free immersion conditions) using a Digital Instruments Nanoscope IIIa Multimode SPM with an n-type doped silicon pyramid single crystal tip coated with PtIr5 (SCM-Pit probe, with a tip radius and height of 20 nm and 10–15 μm, respectively). The local surface potential maps were recorded in the dual-scan mode. In the first scan, topography data were obtained in the dynamic mode (e.g., tapping mode). In the second scan, the tip was lifted to 100 nm, and the surface potential was recorded by following the topography contour registered in the first scan. Both the topography and electrical surface potential maps were captured under ex situ conditions in an air atmosphere at 27 °C and an approximate relative humidity of 28%. In addition, a pixel resolution of 512 × 512, zero-bias voltage, and scan frequency rate of 0.2 Hz were used in all the AFM and SKPFM measurements. To obtain key information regarding the electrical surface potential distribution on a heterogeneous surface, for example, the adsorbed protein nanofilm and its adsorption morphology, histogram

analysis based on multimodal Gaussian distributions was performed according to the procedure followed in previous studies [58,59]. In addition, the microstructural examination of the CoCrMo sample was performed using FE-SEM (JEOL, JSM-7610FPlus, 5 kV, and a working distance of 15 mm) with a secondary electron (SE) detector.

2.3. Electrochemical measurements

2.3.1. Potentiodynamic polarization and applied anodic potential

The electrochemical measurements, including the potentiodynamic polarization (PDP) and applied anodic potential of the CoCrMo alloy, were performed using an AUTOLAB PGSTAT 30 potentiostat instrument in a PBS solution with various BSA concentrations (0, 0.5, and 2 $g{\cdot}L^{-1}$ BSA protein). An $Ag/AgCl/KCl_{3\ M}$ electrode (+222 mV vs. SHE) and platinum wire were used as the reference and counter electrodes, respectively, and the CoCrMo specimen served as the working electrode. The PDP measurements were conducted at a scan rate of 1 $mV.s^{-1}$ from the cathodic to anodic potentials after 1 h immersion in the above environments to reach the steady-state condition and stabilized open circuit potential (OCP). To visualize the semiconductor characteristics of the CoCrMo oxide layer at different passivity potentials, the working electrodes were anodically polarized at +100 mV and +300 mV vs. Ag/AgCl for 1 h in the selected environments, as mentioned above.

2.3.2. Mott-Schottky analysis in BSA protein environments

The semiconductor characteristics of the oxide layer (for e.g., the donor and acceptor charge carriers) on the CoCrMo complex oxide layer were measured in the differently polarized samples, including OCP, + 100 mV, and + 300 mV vs. Ag/AgCl, using different BSA protein concentrations, including 0, 0.5, and 2 $g{\cdot}L^{-1}$, during exposure to PBS solution by the interfacial capacitance (C) versus applied potential (E). The MS analysis can be explained using the following equation [60]:

$$\frac{1}{C^2}=\frac{1}{C_{SC}^2}+\frac{1}{C_H^2}+\frac{1}{C_{Diff}^2}=\pm\frac{2}{\varepsilon\varepsilon_0 eN_{d\ or\ a}}(E-E_{fb}-\frac{kT}{e}), \quad (1)$$

where C_{SC} is the space charge capacitance (SCR), C_H is the capacitance of the Helmholtz double layer, C_{Diff} corresponds to the diffuse layers in the solution, ε is the dielectric constant of the passive film, ε_0 is the vacuum permittivity (8.854×10^{-14} $F.cm^{-1}$), e is the electron charge (1.6×10^{-19} C), N_d is the donor density, N_a is the acceptor density, E_{fb} is the flat band potential, and k and T are the Boltzmann constant and absolute temperature, respectively. It has been proven that the SCR in the topmost part of a semiconductor oxide layer definitely reflects a lower capacitance value than the diffuse layer, particularly the Helmholtz double layer [61,62]. Therefore, the capacitance value in the MS analysis is considered to be almost the SCR of the CoCrMo complex oxide layer. The MS analysis was performed at a frequency of 1 kHz in the potential range of −1 V up to +1 V vs. Ag/AgCl with an amplitude of ± 10 mV in all the selected solutions. It is noteworthy that a frequency of 1 kHz was selected in this study because at frequencies higher than 1 kHz, small variations can be seen in the capacitance values [51,61,63]. In contrast, the non-uniform or heterogeneous protein adsorbed layer (only in the protein environment) on the CoCrMo complex oxide layer can significantly modify the semiconductor characteristics and E_{fb} [64]. Nevertheless, the physicochemical interactions of the protein molecules such as adsorption and detachment (protein or metal-protein species) are dynamic processes, and different potential sweeping on MS can slightly affect these interactions [45,65].

3. Results and discussion

3.1. Morphology and surface potential distribution of various protein concentrations

Using AFM/SKPFM, we visualized the adsorption morphology and electrical surface potential distribution of the adsorbed BSA protein on the CoCrMo oxide surface after 1 h immersion in PBS solution with various BSA concentrations (0, 0.5, and 2 $g{\cdot}L^{-1}$), as presented in Fig. 1. In general, using SKPFM, it is possible to determine the local surface potential or work function energy (*WFE*) distribution on the targeted sites on the substrate without any physical contact between the conductive AFM tip and the specimen surface [18].

As presented in the SKPFM map of CoCrMo in the absence of the BSA protein molecules (Fig. 1d), an approximately homogeneous surface potential distribution along some polished lines on the CoCrMo surface can be observed. Considering the corresponding surface topography image shown in Fig. 1a and the FESEM microstructural image (Fig. S1) of the polished sample, it can be seen that the slight variation in the electrical surface potential in Fig. 1d can be attributed to the grains and twins with various topographies (different polishing behaviors) and surface potential values. However, by adding 0.5 and subsequently 2 $g{\cdot}L^{-1}$ of BSA protein to the PBS solution, the surface microstructure features of the CoCrMo alloy gradually vanished (Fig. 1b and c). Moreover, the surface potential map of the CoCrMo surface in 0.5 and 2 $g{\cdot}L^{-1}$ BSA protein appeared in the form of a heterogeneous surface potential distribution with new surface features that are assigned to the protein denatured and/or fibrillar protein aggregates (Fig. 1e and f). Based on the histogram analysis of the topography maps shown in Fig. 2a and the calculated results presented in Table 1, a slight decrease in both the mean values (μ) of the surface roughness ($\mu_{0\ g/L}=27.5$ nm > $\mu_{0.5\ g/L}=24.5$ nm > $\mu_{2\ g/L}=18.8$ nm) and standard deviations (σ) of the topography ($\sigma_{0\ g/L}=11.2$ nm > $\sigma_{0.5\ g/L}=7.8$ nm > $\sigma_{2\ g/L}=6.2$ nm) were observed for the CoCrMo surface when the BSA protein was increased from 0 up to 2 $g{\cdot}L^{-1}$. These evaluations of the surface roughness in the presence of the BSA protein can be ascribed to the adsorption of protein soft molecules, filling and covering the rough polished surface at the nanometric scale. As shown in the histograms of the electrical surface potential images in Fig. 2b and Table 1, it can be seen that increasing the BSA protein concentration caused a shift in the overall electrical surface potential distribution (protein and substrate) to lower values.

It is known that the adsorbed protein and DNA biological molecules on metal and oxide surfaces exhibit a lower electrical surface potential value than the matrix [32,66], which was also investigated in our previous studies [19,51] (vide infra). Hence, considering this point, we can infer that increasing the BSA concentration from 0 up to 2 $g{\cdot}L^{-1}$ triggered a decrease in the overall electrical surface potential distribution ($\mu_{0\ g/L}=16.4$ nm > $\mu_{0.5\ g/L}=11.9$ nm > $\mu_{2\ g/L}=10.8$ nm, Table 1) on the oxide surface due to more BSA protein coverage, resulting in a greater hindering impact on the electrostatic interaction between the tip and oxide surface [19].

We further investigated the nanometric scale using AFM/SKPFM for a more precise understanding of some crucial information, including the adsorption shape and covering level of various protein concentrations, as well as the electrical surface potential and energy level diagram of a single BSA protein, as shown in Figs. 3 and 4. Comparing the AFM maps of the CoCrMo surface for all BSA concentrations at 500 × 500 nm^2 (Fig. 3a–c), we can discern that the sample with 2 $g{\cdot}L^{-1}$ BSA concentration displays a more protein surface covering, increasing with either the thickness of the adsorbed protein film and standard deviation values. Indeed, based on the histogram analysis of the topography maps shown in Fig. 3d and Table 1, both the mean value of the height and standard deviation values on CoCrMo oxide surface were enhanced by increasing the BSA protein concentration.

Albumin is a plasma protein that is present in high concentrations in the synovial fluid, particularly on the adsorption surface [1]. The dimensions of the BSA molecule are 4 nm × 4 nm × 14 nm with an ellipsoidal shape [6]. Based on this and the topography histogram results shown in Fig. 3d, we can observe that at 0.5 $g{\cdot}L^{-1}$ BSA concentration, the tendency of the BSA protein to undergo denaturation on the CoCrMo surface is higher than that at 2 $g{\cdot}L^{-1}$ BSA concentration.

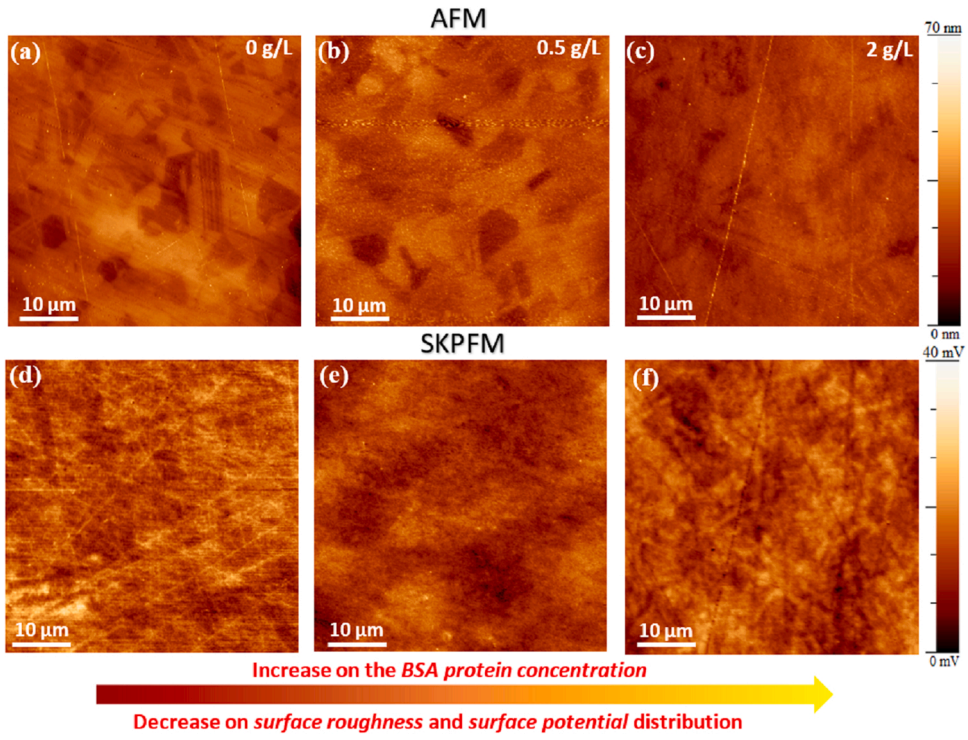

Fig. 1. Topography and electrical surface potential images of the CoCrMo surface exposed to PBS solution with different BSA concentrations including (a and d) 0, (b and e) 0.5, and (c and f) 2 g·L^{-1} at 37 °C, pH 7.4, and under aerated conditions.

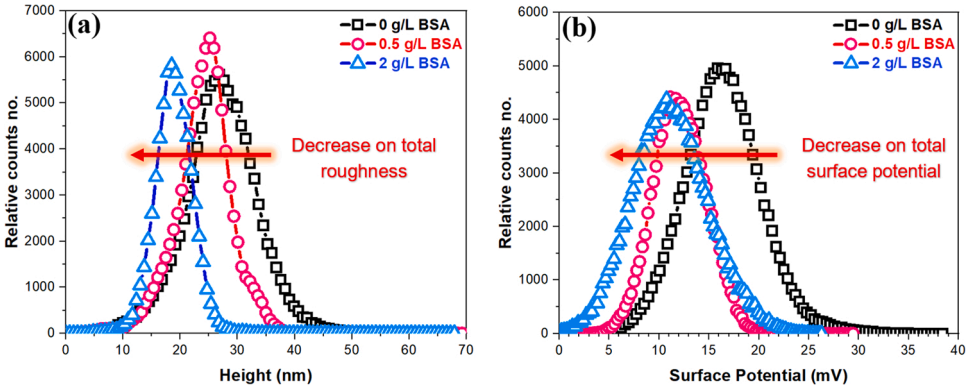

Fig. 2. (a) Topography and (b) electrical surface potential histogram analyses extracted from the topography and surface potential images shown in Fig. 1.

Table 1
Extracted Gaussian distribution parameters from the topography and surface potential histograms in Figs. 2 and 3.

Concentration	0 g/L BSA	0.5 g/L BSA	2 g/L BSA
Constituents	Substrate	Substrate+protein	Substrate+protein
Mean value of Topography-Fig. 2a	27.5 ±11.2 nm	24.5 ± 7.8 nm	18.8 ± 6.2 nm
Mean value of Topography-Fig. 3d	3.4 ±1.2 nm	3.7 ± 1.4 nm	4.1 ± 1.7 nm
Mean value of Surface potential-Fig. 2b	16.4 ±6.8 mV	11.9 ± 6.1 mV	10.8 ± 7.8 mV

Indeed, at high BSA protein concentrations, the BSA protein nanofilm exhibits a more globular adsorption shape with a slightly elongated feature that is very close to the BSA dimensional model (4 nm–4.1 nm, our results). The SKPFM image of the adsorbed BSA nanofilm shown in Fig. 3f, which corresponds to the AFM image shown in Fig. 3c, clearly confirms a lower electrical surface potential distribution in the BSA protein region than on the CoCrMo oxide surface. Hence, these AFM/SKPFM findings reveal that a concentration of 2 g·L^{-1} compared with 0.5 g·L^{-1} facilitates the formation of a perfect protein nanofilm (lower denatured shape) on the CoCrMo surface with a particular globular shape and the lowest electrical surface potential, which in turn directly influences the electrochemical interactions, electrical double layer, and charge transfer process at the electrolyte/protein/oxide interface. Nevertheless, the mechanism by which the protein molecules affect the energy level diagram and in turn the electrical surface potential on the protein/oxide interface in a solid-state condition remains to be determined. To address this, further elucidation was performed using high-resolution AFM/SKPFM on a single BSA protein and the corresponding energy level diagram, which is discussed in detail in the next section.

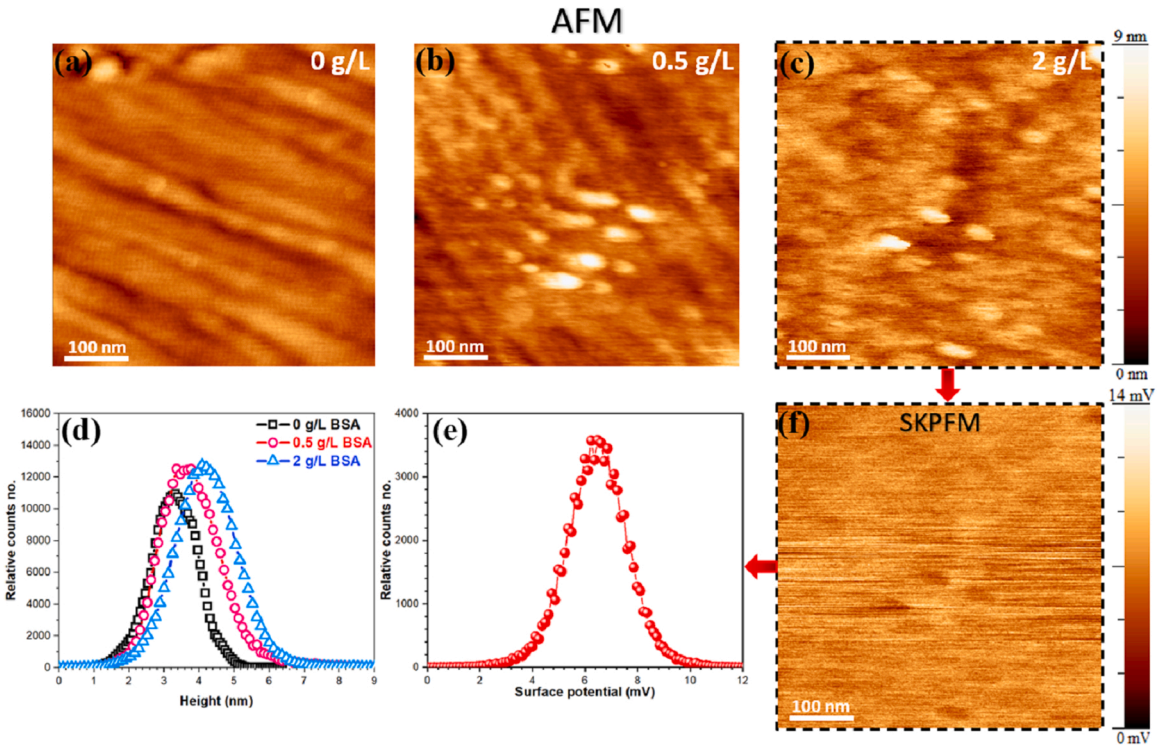

Fig. 3. Topography images of the CoCrMo samples exposed to PBS solution for 1 h with various BSA concentrations including (a) 0 g·L^{-1}, (b) 0.5 g·L^{-1}, and (c) 2 g·L^{-1} BSA protein at 37 °C, pH 7.4, and under aerated conditions. (d) Topography histogram analysis derived from (a, b, and c). (e) Surface potential histogram analysis corresponding to (f). (f) Local surface potential image corresponding to the topography image in (c).

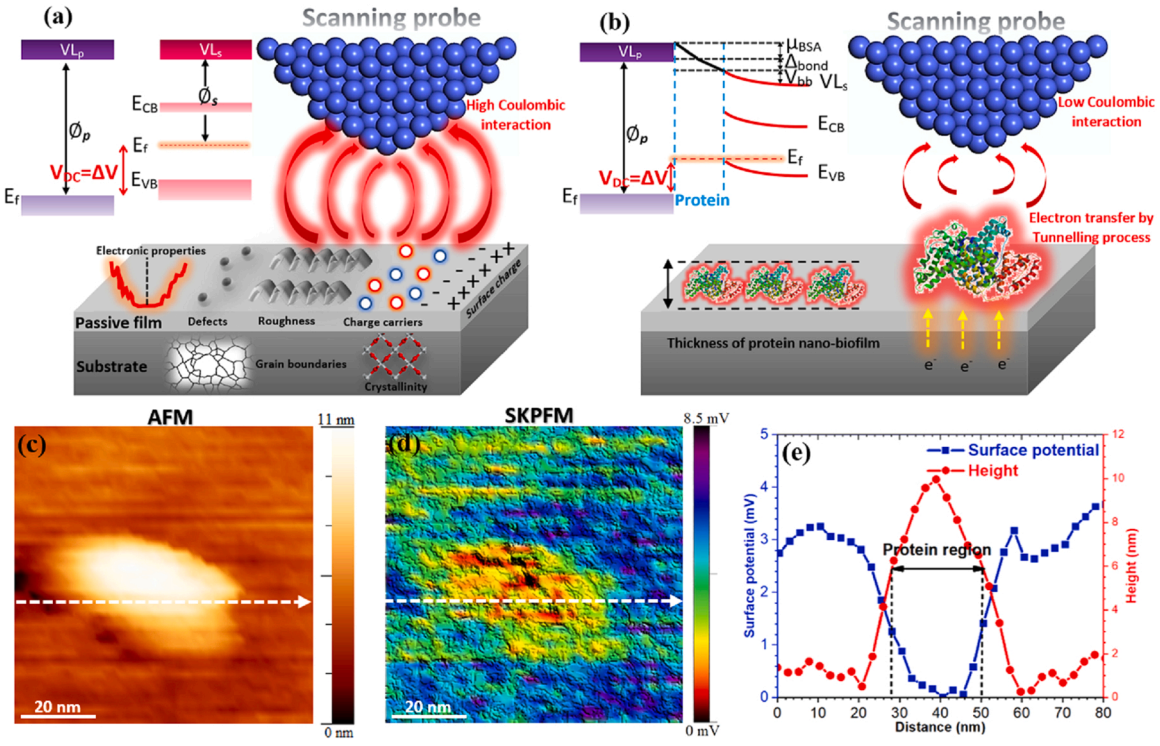

Fig. 4. (a) Schematic illustration of the SKPFM principle together with the energy levels during electrostatic interaction between the conductive probe and semiconductor oxide film/bulk materials at the atomic scale. (b) The presence of a single adsorbed protein that significantly modifies the energy levels and total surface potential difference. (c) AFM and (d) SKPFM images of a single BSA molecule on the CoCrMo surface during 1 h immersion of the CoCrMo surface in PBS +2 g·L^{-1} BSA environment at 37 °C, pH 7.4, and under aerated conditions. (e) Topography and local surface potential line profiles of a single BSA molecule extracted from (c) and (d).

3.2. Nanometric/atomistic approach to the energy level evaluations at the protein/oxide interface using SKPFM

At a constant bias voltage and tip-sample distance in the SKPFM technique, the recorded *WFE* values correspond to the electrical surface potential difference (ΔSP) between the conductive probe and the considered substrate as [27]:

$$\Delta SP = \left(\varnothing_p - \varnothing_s\right)/e, \quad (2)$$

where e is the elementary charge, and $\varnothing_p$ and $\varnothing_s$ are the *WFEs* of the probe and substrate, respectively. In addition, the schematic shown in Fig. 4a demonstrates the basic principle of the SKPFM technique along with the energy levels (for e.g., the valence and conduction bands (E_{VB} and E_{CB}), Fermi level (E_f), and vacuum level (VL) of the probe and substrate).

It is essential to mention that in a simple or complex system of semiconductor or dielectric materials, the surface potential or electrostatic interactions strongly correlate with the entire WFEs, static charges, and multipoles of the surface components [32,67,68]. For example, the electrical surface potential signal on the oxide layer of the CoCrMo alloy with a heterogeneous distribution of various oxide components results from the sum of the weighted concentrations of the *WFEs* of the oxide constituents, which in this case is given by $WFE_{total} = \varnothing_{pCr2O3} + \varnothing_{pCoO} + \varnothing_{pMoO3}$ [19,40]. However, some crucial chemical and physical characteristics of the oxide layer and bulk material, such as the surface roughness, defects, charge distribution, charge carriers, surface energy, crystallinity, and valence and conductance states, considerably influence the electrostatic interactions and charge transfer process, particularly at the protein nano-biofilm/oxide layer interface [19,45], as shown in Fig. 4a and b.

It is well known that the adsorption of monolayers or multilayers of organic molecules, such as the chemisorbed self-assembled monolayers, Langmuir-Blodgett film, and even proteins and DNAs, remarkably affects the measured surface potential (SP_{Oxide}) [69,70], as schematically illustrated in Fig. 4b for a single BSA molecule on the oxide surface. This figure shows that the adsorbed BSA molecule on the surface oxide induces the alternation of the surface energy levels and subsequently the intensity of the electrostatic interaction between the conductive tip and adsorbed BSA on the oxide layer. Because of this, the energy band diagram on the protein molecule side shows band bending (V_{bb}), which alters the effective molecular dipole (μ_{BSA}) and interface dipoles (Δ_{bond}) due to the BSA/oxide layer interface interaction (Fig. 4b). These evaluations in the energy band diagram originate from the new arrangement and amount of charge carriers in the adsorbed BSA region on the oxide layer [7,27,47]. Therefore, the total magnitude of the electrical surface potential on the BSA molecule-complex oxide (SP_{surf}) can be described as [27].

$$SP_{surf} = SP_{Oxide} + \mu_{BSA}/e + \Delta_{bond}, \quad (3)$$

It is worth mentioning that the formation of a thick organic film (>100 nm) on the surface oxide layer significantly hinders the effect of the bulk material on the magnitude of SP_{surf} because of the limited range of interactions between the tip and the surface [27,70].

To visualize a realistic surface potential signal from the adsorbed BSA protein on the CoCrMo oxide surface, AFM and SKPFM surface maps of a single BSA protein molecule were obtained at nanoscale resolution, as presented in Fig. 4c and d. These high-resolution topography and electrical surface potential maps were captured after 1 h exposure of the CoCrMo sample to PBS+ 2 $g{\cdot}L^{-1}$ BSA solution at 37 °C and pH ~7.4. According to the topography image and line profile depicted in Fig. 4c and e, the adsorbed single BSA protein has an ellipsoidal shape with an approximate height of ~10 nm. An apparent longer dimension of a single BSA molecule with respect to the standard BSA dimensions, for example, 4 nm × 4 nm × 14 nm, is possibly related to the AFM tip-sample convolutions [6].

In addition, these images depict a BSA molecule's desaturated structure with a heterogeneous surface potential and/or charge distribution on its molecular structure [3]. The surface potential of biological molecules strongly depends on the charge distribution and polar residue structure, especially the pH and isoelectric point (IEP) [56]. The IEP defines the pH value at which the protein surface charge has a minimum value, or is zero. In this regard, at solution pH values above and below the IEP, the protein's overall charge is negative and positive, respectively. The IEP value of the BSA protein based on both theoretical estimation and experimental analysis is between 4.7 and 5.4 [7,19]. Moreover, the line profile of the electrical surface potential shown in Fig. 4e indicates a lower electrical surface potential distribution on the BSA molecule structure compared with the complex oxide layer on CoCrMo, with a difference of ~3.5 mV. As stated earlier, the BSA molecule with chemisorb adsorption on the CoCrMo oxide layer reduced the electrical surface potential due to the presence of new potential steps and band bending at the energy level. Therefore, this surface potential difference at the nanoscale completely elucidates the hindering effect of the BSA protein on the surface potential/charge distribution, which in turn directly influences the electrochemical interaction at the BSA molecule/oxide layer interface, which is discussed in the next section.

3.3. Effect of the protein on the space charge capacitance and corrosion/biodegradation processes

The results of the AFM and SKPFM investigations at the solid/air interface demonstrated that the electrical surface potential of the BSA protein and its nanofilm thickness can remarkably interfere with the electrical properties and charge transfer evaluations of the surface oxide layer (by reducing the electrostatic interactions). Nevertheless, it is still important to visualize the effects of the BSA protein on the semiconductor charge carriers, surface oxide energy levels, and particularly the gradual deterioration of the surface oxide layer at the electrolyte/protein/oxide interface. Correspondingly, it has been reported that physiologically, the potential value of the CoCrMo alloy in the complex human environment can meaningfully shift from the corrosion potential and/or open circuit potential of −0.1 V or −0.2 V reported in this study (Fig. S2) up to + 0.65 V (transpassive region) due to the presence of the H_2O_2 agent and Fenton reactions as the inflammatory conditions [42]. Therefore, MS analysis was conducted on the CoCrMo specimens after 1 h immersion in PBS solution containing various BSA concentrations (0, 0.5, and 2 $g{\cdot}L^{-1}$) and at different applied overpotentials (OCP, +100 mV, and +300 mV vs. Ag/AgCl anodically polarized (Fig. S2)), as shown in Fig. 5.

Depending on the different applied overpotentials, two individual regions were marked/identified in the MS analysis based on the slopes of the curves (the positive and negative slopes correspond to the n-type and p-type semiconductor characteristics, respectively [60]), including region I with n-type semiconductor behavior (donor density) and region II with p-type semiconductor (acceptor density) behavior. The CoCrMo oxide layer in region I under the OCP condition (Fig. 5a) exhibits different slopes during sweeping at different applied potentials (−1 V to +1 V vs. Ag/AgCl).

According to the literature, various hypotheses have been proposed for these multiple apparent slopes, including the presence of surface states [33,51], inhomogeneous distribution of the donor charge carriers [60], and dependency of the type and density of the donor charge carriers on the sweeping potential [71]. Therefore, in the case of the CoCrMo alloy, this comes from new evaluations of the chemical composition and donor density distribution within the complex oxide film, especially in Cr oxides [72]. Indeed, at potentials lower than + 0.3 V vs. Ag/AgCl or region I, Cr appears in two different forms, including Cr_2O_3 and $CrOH_3$, which were detected using XPS analysis with a significant presence of OH^- in the O1s peaks [72,73]. However, when we shift from region I (passive film) to region II (transpassive oxidation) approximately after + 0.3 V vs. Ag/AgCl, the intensive

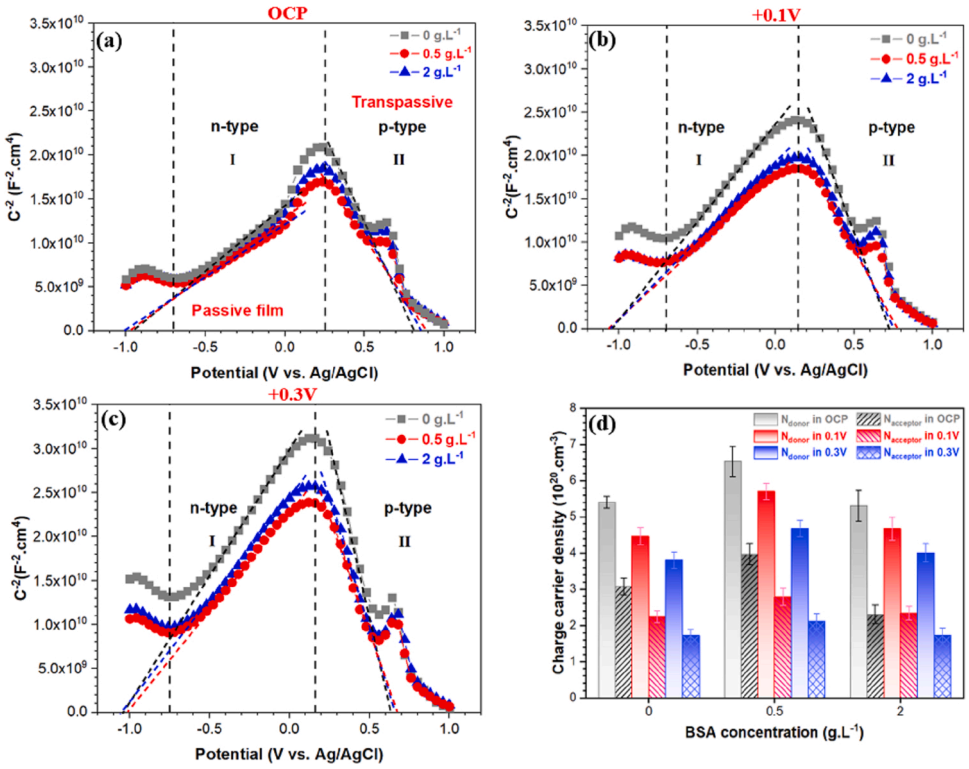

Fig. 5. Mott-Schottky analysis of the CoCrMo alloy after 1 h immersion in PBS, PBS +0.5 g·L^{-1} BSA, and PBS +2 g·L^{-1} environments at (a) OCP, (b) +100 mV, and (c) +300 mV vs. Ag/AgCl overpotential conditions at 37 °C, pH 7.4, and under aerated conditions. (d) Donor and acceptor carrier densities in the complex oxide layer of CoCrMo under different environments and applied anodic potentials analyzed from (a), (b), and (c).

release of Cr and Mo ions mainly accompanies the formation of more complexes with phosphate species [72]. The results from the PDP curves shown in Fig. S2 further confirm the gradual deterioration of the passive film at potentials higher + 0.3 V vs. Ag/AgCl in all environments. In region II, the Cr and Mo ions tend to precipitate in the passive film as hydrated oxides or oxychlorides, and the Co ions remain solvated in solution [40].

The polarized samples (+100 mV and +300 mV vs. Ag/AgCl) clearly indicate an enhancement of the C^{-2} magnitude and a more smoothing behavior on the curve slopes in region I compared with the OCP condition, which reaches the highest C^{-2} magnitude at + 300 mV vs. Ag/AgCl polarization. Hence, the continuous growth of the oxide layer during polarization gradually affected the thickness, compacting, and charge carriers of the oxide layer [51]. It can be seen from the MS curves that the BSA protein environments decreased the C^{-2} magnitude in all regions along with a slight decrease in the linear slope in region I in the OCP and polarized samples. Moreover, by changing the BSA concentrations from 2 to 0.5 g·L^{-1} in all the solutions, both the C^{-2} magnitude and linear slope reached the lowest values. This trend can be attributed to the adsorption of the BSA protein on the passive film, which affects the SCR, especially the distribution of the charge carrier densities. To calculate the donor (N_d) and acceptor (N_a) densities, the value of ε was considered to be 13, in agreement with previous studies [74]. The N_d (region I) and N_a (region II between +0.25 V up to +0.5 V vs. Ag/AgCl) were calculated by fitting a straight line to the linear portion of the slopes according to the following equation [75]:

$$\alpha = \frac{-2}{N_d or N_a e \varepsilon \varepsilon_0}, \quad (4)$$

where α is the slope of C^{-2} versus the applied potential.

The calculated N_d and N_a results shown in Fig. 5d reveal that the polarized sample at + 300 mV vs. Ag/AgCl presents the lowest value of the donor and acceptor charge carriers with respect to the other conditions in the + 300 mV< +100 mV< OCP condition. By changing the BSA protein concentration from 0.5 to 2 g·L^{-1}, the density of charge carriers within the passive film decreased in all the samples. This occurrence can be ascribed to the hindering of the electrochemical interactions (charge transfer through the passive film and passive film growth) and/or effect on the surface states due to a thick or dense nanolayer of the BSA protein. Nevertheless, according to the PDP curves in Fig. S2 and electrochemical impedance spectroscopy (EIS) analysis presented in Fig. S3 and Table S1, this postulation was further confirmed as the 2 g·L^{-1} BSA compared with the 0.5 g·L^{-1} concentration reduced both the corrosion and passivity current densities and also enhanced on total impedance value of CoCrMo alloy. Therefore, a lower tendency for charge transfer can be anticipated on the film formed in 2 g·L^{-1} BSA than in 0.5 g·L^{-1} over the CoCrMo oxide layer, leading to a reduction in the electrochemical interactions and/or metal ion release process. This result is in accordance with the AFM and SKPFM visualizations, which revealed the higher surface coverage of the BSA protein in 2 g·L^{-1} BSA solution compared with 0.5 g·L^{-1}, thus allowing a less denatured molecular structure to decrease the total electrical surface potential on the CoCrMo surface. It is essential to highlight that the CoCrMo alloy, during exposure to only PBS media under all the overpotential conditions (OCP, +100 mV, and +300 mV vs. Ag/AgCl), presented the lowest values of both the corrosion and passivity current densities, as well as the donor charge carriers (Figs. 5d and S2). This is undoubtedly related to the significant role of HPO_4^{2-} and $H_2PO_4^-$ as the dominant species in the PBS media that can easily adsorb onto the CoO, Cr_2O_3, and MoO_3 oxides to form a thin phosphate-complex film, which hinders the release of the Co, Cr, and Mo ions or blocks the mass transport compared to the PBS+BSA environment [51]. As reported in the literature, the adsorbed protein on TiO_2 oxide can shift the flat band potential (E_{fb}) to more negative values and increase N_d due to local alkalization of the (hydr)oxide surface groups on TiO_2 [52]. In fact, the adsorbed layer of BSA proteins can strongly affect the SCR, which is directly related to the charge carrier

density in the conduction band [52].

It is worth noting that at the CoCrMo surface oxide (mainly Cr_2O_3), oxygen vacancies give rise to occupied electron energy levels below the conduction band of the semiconductor oxide and, in turn, act as appropriate sites for the adsorption of simple molecules [64]. Moreover, the presence of dangling bonds in the surface atoms can generate localized electron energy levels at the interface. In this regard, any evaluation of the surface states can directly affect the electronic properties of the semiconductor oxide and interfacial electrical double layer [52], as presented in the SKPFM section. In addition, the interaction of the ions and/or molecular species (here BSA protein) through physi-chemisorption processes with the oxide surface can lead to the formation of exterior surface states. Hence, the adsorption of BSA molecules on the complex oxide layer of CoCrMo leads to occupied electron energy levels in the oxide bandgap energy, thereby increasing N_d by introducing exterior surface states and shifting E_{ft} to negative values. These descriptions are in accordance with the summarized theoretical relationship between the flat band potential and N_d, and can be expressed as follows [64]:

$$E_{ft} = a - 2.303\frac{kT}{e} log N_d, \quad (5)$$

where a is a constant. Consequently, the shift of the C^{-2} magnitude to lower values in BSA protein environments can be attributed to the chemical modification of the oxide surface due to sharper band bending or upward shifting and increase in the SCR thickness [64], as shown schematically in Fig. 6a and b.

It is worth mentioning that the surface conformation of the protein molecules in the form of a side-on or end-on position interferes with the number of interaction sites between the protein and oxide surface, resulting in a significant impact on the capacitance value at the protein/oxide interface [64,76]. The BSA adsorbed on the CoCrMo oxide surface is mainly in a side-on orientation with respect to the end-on position, as revealed by AFM in Fig. 3, and thus the formed protein nanofilm generates a lower number of adsorbed protein molecules per surface unit and smaller surface area at the protein/oxide interface. From a corrosion point of view, the low donor density explains the electrochemical reactions at the oxide/solution interface, which can be inhibited by reducing the charge transfer (also confirmed by the SKPFM and PDP analyses). The intensity of N_d is related to the density of the oxygen vacancies or interstitial distribution of Co, Cr, and Mo in the passive film region [75]. Thus, the decrease in the formation rate and transfer velocity of oxygen vacancies along with metal interstitials enhances the stability and protective behavior of the passive film with low mass transfer [77]. As a result, we can state that a low BSA protein concentration provides more exterior surface states, a higher dissolution rate owing to the increase in the number of defect sites, and a higher rate of mass transport through the oxide region, decreasing the protective properties in accordance with the SKPFM and PDP analyses results. These results are also in agreement with a previous study that confirmed that CoCrMo at high BSA protein concentrations with respect to lower amounts in PBS solution presents a low corrosion rate (calculated using EIS and PDP analyses) [54] and metal ion release during long-term monitoring (analyzed with an induced coupled plasma-optical emission spectrometer (ICP-OES)) [78]. Finally, we summarized all our investigations in this study and present a schematic representation to better describe the impact of different protein concentrations and applied overpotential conditions on the corrosion/biodegradation mechanisms on the oxide surface of the CoCrMo alloy, as shown in Fig. 7.

4. Conclusions

In summary, this study provided new approaches to investigating the relationship between the electrical surface potential of adsorbed BSA protein films and the evolution of the electronic properties of the CoCrMo oxide layer at the protein/oxide interface for corrosion/biodegradation mechanisms. Using SKPFM, it was shown that the BSA protein nanofilm with a higher thickness obtained at a concentration of 2 $g{\cdot}L^{-1}$ can remarkably decrease the electrostatic surface potential or surface charge distribution on the CoCrMo oxide layer, resulting in a lower tendency for charge transfer at the protein/electrolyte interface. Using potentiodynamic polarization, it was confirmed that the 2 $g{\cdot}L^{-1}$ BSA protein, compared with a 0.5 $g{\cdot}L^{-1}$ concentration, better hinders the charge transfer (lower corrosion and passivity current densities) for electrochemical interactions at the protein/electrolyte interface. In particular, the MS analysis at the electrolyte/protein/oxide interface demonstrated that the adsorbed protein film obtained at 0.5 $g{\cdot}L^{-1}$ more than that obtained at 2 $g{\cdot}L^{-1}$ concentration can significantly enhance the n- and p-type charge carriers and space charge capacitance values due to increased band bending at the space charge region/protein interface. Indeed, a reduction in the metal ion release process of metallic biomaterials in protein media can be achieved at high protein concentrations with respect to lower concentrations because of the lower electrical surface potential of the protein nanofilm (surface charge on the protein), lower corrosion and passivity current density, and lower charge carrier distribution through the oxide surface exposed to the electrolyte.

CRediT authorship contribution statement

Ehsan Rahimi: Methodology, Investigation, Writing – original draft. **Ruben Offoiach:** Methodology, Investigation, Writing – review & editing. **Maria Lekka:** Methodology, Writing – review & editing, Resources, Funding acquisition, Supervision, Project administration. **Lorenzo Fedrizzi:** Writing – review & editing, Resources, Funding acquisition, Supervision, Project administration.

Declaration of Competing Interest

The authors declare that they have no known competing financial interests or personal relationships that could have appeared to influence

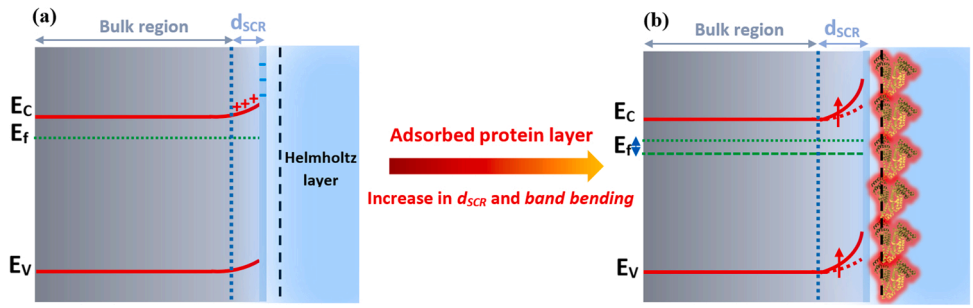

Fig. 6. Schematic representation of the energy band diagrams for (a) an n-type semiconductor oxide film/electrolyte interface, and (b) adsorption of protein molecules on the oxide layer to form a nano-biofilm, which finally results in an increase in both the band bending and SCR thickness.

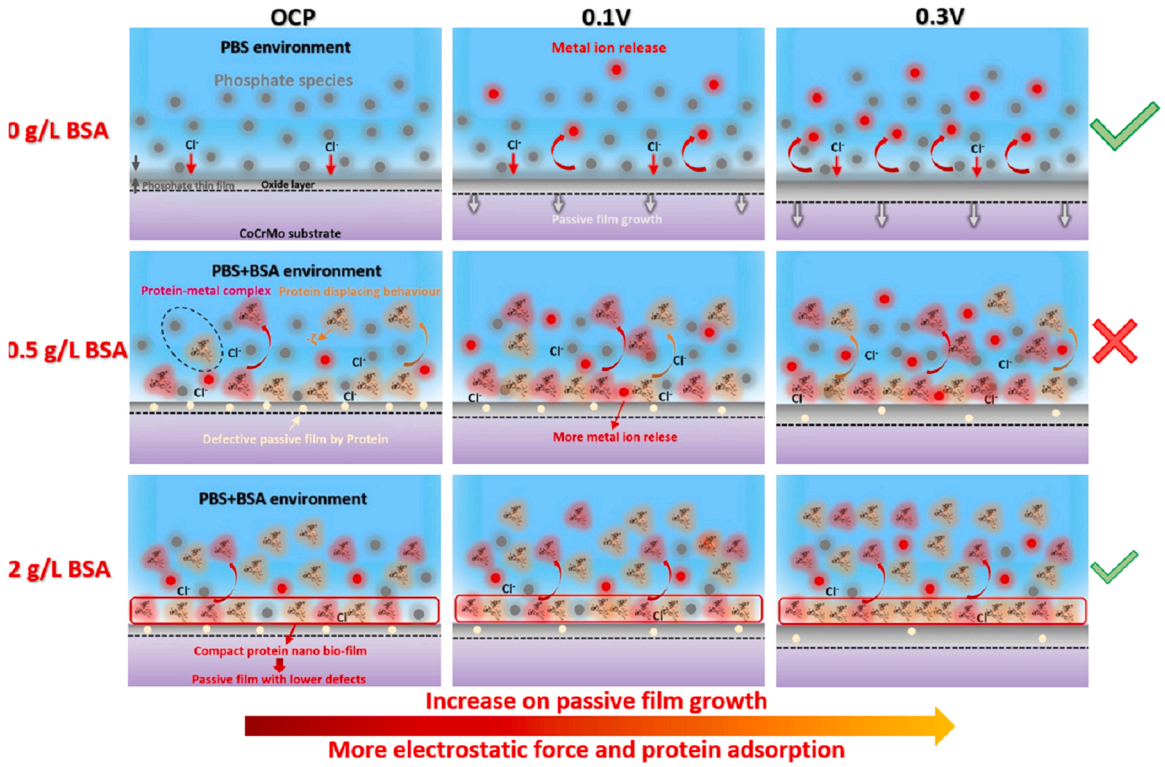

Fig. 7. Schematic representation of the impact of different BSA protein concentrations and applied anodic potentials on the BSA protein adsorption, metal ion release, and defect/charge carrier distribution on the CoCrMo oxide film. The large red arrow indicates an increase in both the passive film growth and protein adsorption upon application of an anodic overpotential. The large green sign, small green sign, and red sign present the best corrosion performance of the alloy in PBS media, medium corrosion performance, and very weak corrosion performance in an aggressive condition, respectively.

the work reported in this paper.

Acknowledgements

This project has received funding from the European Union's Horizon 2020 research and innovation program under the Marie Sklodowska-Curie grant agreements No 764977. University of Udine, Italy is appreciated for providing all microscopy and electrochemical setups.

Appendix A. Supporting information

Supplementary data associated with this article can be found in the online version at doi:10.1016/j.colsurfb.2022.112346.

References

[1] Y.S. Hedberg, Role of proteins in the degradation of relatively inert alloys in the human body, npj Mater. Degrad. 2 (1) (2018) 26.
[2] S. Hiromoto, T. Hanawa, pH near cells on stainless steel and titanium, Electrochem. Solid State Lett. 7 (3) (2004) B9–B11.
[3] Y. Jeyachandran, E. Mielczarski, B. Rai, J. Mielczarski, Quantitative and qualitative evaluation of adsorption/desorption of bovine serum albumin on hydrophilic and hydrophobic surfaces, Langmuir 25 (19) (2009) 11614–11620.
[4] M. Talha, Y. Ma, P. Kumar, Y. Lin, A. Singh, Role of protein adsorption in the bio corrosion of metallic implants–A review, Colloids Surf. B Biointerfaces (2019).
[5] S. Guo, D. Pranantyo, E.-T. Kang, X.J. Loh, X. Zhu, D. Jańczewski, K.G. Neoh, Dominant albumin–surface interactions under independent control of surface charge and wettability, Langmuir 34 (5) (2018) 1953–1966.
[6] I. Ron, L. Sepunaru, S. Itzhakov, T. Belenkova, N. Friedman, I. Pecht, M. Sheves, D. Cahen, Proteins as electronic materials: Electron transport through solid-state protein monolayer junctions, J. Am. Chem. Soc. 132 (12) (2010) 4131–4140.
[7] Y. Yan, H. Yang, Y. Su, L. Qiao, Albumin adsorption on CoCrMo alloy surfaces, Sci. Rep. 5 (2015) 18403.
[8] M. Talha, Y. Ma, Y. Lin, A. Singh, W. Liu, X. Kong, Corrosion behaviour of austenitic stainless steels in phosphate buffer saline solution: synergistic effects of protein concentration, time and nitrogen, New J. Chem. 43 (4) (2019) 1943–1955.
[9] E. Rahimi, R. Offoiach, S. Deng, X. Chen, S. Pané, L. Fedrizzi, M. Lekka, Corrosion mechanisms of magnetic microrobotic platforms in protein media, Appl. Mater. Today 24 (2021), 101135.
[10] R. Gulaboski, V. Mirčeski, I. Bogeski, M. Hoth, Protein film voltammetry: electrochemical enzymatic spectroscopy: a review on recent progress, J. Solid State Electrochem. 16 (7) (2012) 2315–2328.
[11] M.T. Stankovich, A.J. Bard, The electrochemistry of proteins and related substances part III. Bovine serum albumin, J. Electroanal. Chem. Interfacial Electrochem. 86 (1) (1978) 189–199.
[12] I. Ron, I. Pecht, M. Sheves, D. Cahen, Proteins as solid-state electronic conductors, Acc. Chem. Res. 43 (7) (2010) 945–953.
[13] N.L. Ing, R.K. Spencer, S.H. Luong, H.D. Nguyen, A.I. Hochbaum, Electronic conductivity in biomimetic α-helical peptide nanofibers and gels, ACS Nano 12 (3) (2018) 2652–2661.
[14] Q. Chi, O. Farver, J. Ulstrup, Long-range protein electron transfer observed at the single-molecule level: In situ mapping of redox-gated tunneling resonance, Proc. Natl. Acad. Sci. USA 102 (45) (2005) 16203–16208.
[15] E.A.D. Pia, Q. Chi, D.D. Jones, J.E. Macdonald, J. Ulstrup, M. Elliott, Single-molecule mapping of long-range electron transport for a cytochrome b 562 variant, Nano Lett. 11 (1) (2010) 176–182.
[16] B. Zhang, S. Lindsay, Electronic decay length in a protein molecule, Nano Lett. 19 (6) (2019) 4017–4022.
[17] J. Zhao, J.J. Davis, M.S. Sansom, A. Hung, Exploring the electronic and mechanical properties of protein using conducting atomic force microscopy, J. Am. Chem. Soc. 126 (17) (2004) 5601–5609.
[18] V. Palermo, A. Liscio, M. Palma, M. Surin, R. Lazzaroni, P. Samorì, Exploring nanoscale electrical and electronic properties of organic and polymeric functional materials by atomic force microscopy based approaches, Chem. Commun. 32 (2007) 3326–3337.
[19] E. Rahimi, R. Offoiach, S. Hosseinpour, A. Davoodi, K. Baert, A. Lutz, H. Terryn, M. Lekka, L. Fedrizzi, Effect of hydrogen peroxide on bovine serum albumin adsorption on Ti6Al4V alloy: a scanning Kelvin probe force microscopy study, Appl. Surf. Sci. (2021), 150364.
[20] C. Shih, A.K. Museth, M. Abrahamsson, A.M. Blanco-Rodriguez, A.J. Di Bilio, J. Sudhamsu, B.R. Crane, K.L. Ronayne, M. Towrie, A. Vlček, Tryptophan-accelerated electron flow through proteins, Science 320 (5884) (2008) 1760–1762.
[21] D. Xu, G.D. Watt, J.N. Harb, R.C. Davis, Electrical conductivity of ferritin proteins by conductive AFM, Nano Lett. 5 (4) (2005) 571–577.
[22] B. Moores, F. Hane, L. Eng, Z. Leonenko, Kelvin probe force microscopy in application to biomolecular films: frequency modulation, amplitude modulation, and lift mode, Ultramicroscopy 110 (6) (2010) 708–711.
[23] J. Park, S. Lee, K. Jang, S. Na, Ultra-sensitive direct detection of silver ions via Kelvin probe force microscopy, Biosens. Bioelectron. 60 (2014) 299–304.

[24] M. Porti, S. Gerardin, M. Nafría, X. Aymerich, A. Cester, A. Paccagnella, P. Schiavuta, R. Pierobon, Systematic characterization of soft- and hard-breakdown spots using techniques with nanometer resolution, Microelectron. Eng. 84 (9) (2007) 1956–1959.
[25] U. Gysin, E. Meyer, T. Glatzel, G. Günzburger, H.R. Rossmann, T.A. Jung, S. Reshanov, A. Schöner, H. Bartolf, Dopant imaging of power semiconductor device cross sections, Microelectron. Eng. 160 (2016) 18–21.
[26] P.B. Hoffmann, A.G. Gagorik, X. Chen, G.R. Hutchison, Asymmetric surface potential energy distributions in organic electronic materials via kelvin probe force microscopy, J. Phys. Chem. C 117 (36) (2013) 18367–18374.
[27] A. Liscio, V. Palermo, P. Samorì, Nanoscale quantitative measurement of the potential of charged nanostructures by electrostatic and Kelvin probe force microscopy: unraveling electronic processes in complex materials, Acc. Chem. Res. 43 (4) (2010) 541–550.
[28] K. Nam, K. Eom, J. Yang, J. Park, G. Lee, K. Jang, H. Lee, S.W. Lee, D.S. Yoon, C. Y. Lee, Aptamer-functionalized nano-pattern based on carbon nanotube for sensitive, selective protein detection, J. Mater. Chem. 22 (44) (2012) 23348–23356.
[29] D.N. Richards, D.Y. Zemlyanov, R.M. Asrar, Y.Y. Chokshi, E.M. Cook, T.J. Hinton, X. Lu, V.Q. Nguyen, N.K. Patel, J.R. Usher, DNA immobilization on GaP (100) investigated by kelvin probe force microscopy, J. Phys. Chem. C 114 (36) (2010) 15486–15490.
[30] H. Lee, S.W. Lee, G. Lee, W. Lee, K. Nam, J.H. Lee, K.S. Hwang, J. Yang, H. Lee, S. Kim, Identifying DNA mismatches at single-nucleotide resolution by probing individual surface potentials of DNA-capped nanoparticles, Nanoscale 10 (2) (2018) 538–547.
[31] A.K. Sinensky, A.M. Belcher, Label-free and high-resolution protein/DNA nanoarray analysis using Kelvin probe force microscopy, Nat. Nanotechnol. 2 (10) (2007) 653.
[32] C. Leung, H. Kinns, B.W. Hoogenboom, S. Howorka, P. Mesquida, Imaging surface charges of individual biomolecules, Nano Lett. 9 (7) (2009) 2769–2773.
[33] E. Rahimi, A. Rafsanjani-Abbasi, A. Imani, A. Davoodi, TiO2/Cu2O coupled oxide films in Cl− ion containing solution: Volta potential and electronic properties characterization by scanning probe microscopy, Mater. Chem. Phys. 212 (2018) 403–407.
[34] A.I. Muñoz, S. Mischler, Interactive effects of albumin and phosphate ions on the corrosion of CoCrMo implant alloy, J. Electrochem. Soc. 154 (10) (2007) C562–C570.
[35] L. Reclaru, P.-Y. Eschler, R. Lerf, A. Blatter, Electrochemical corrosion and metal ion release from Co-Cr-Mo prosthesis with titanium plasma spray coating, Biomaterials 26 (23) (2005) 4747–4756.
[36] K. Yamanaka, M. Mori, I. Kartika, M.S. Anwar, K. Kuramoto, S. Sato, A. Chiba, Effect of multipass thermomechanical processing on the corrosion behaviour of biomedical Co–Cr–Mo alloys, Corros. Sci. (2018).
[37] C.V. Vidal, A.I. Muñoz, Electrochemical characterisation of biomedical alloys for surgical implants in simulated body fluids, Corros. Sci. 50 (7) (2008) 1954–1961.
[38] B. Stojanović, C. Bauer, C. Stotter, T. Klestil, S. Nehrer, F. Franek, M.R. Ripoll, Tribocorrosion of a CoCrMo alloy sliding against articular cartilage and the impact of metal ion release on chondrocytes, Acta Biomater. 94 (2019) 597–609.
[39] A. Ouerd, C. Alemany-Dumont, B. Normand, S. Szunerits, Reactivity of CoCrMo alloy in physiological medium: Electrochemical characterization of the metal/protein interface, Electrochim. Acta 53 (13) (2008) 4461–4469.
[40] I. Milošev, The effect of biomolecules on the behaviour of CoCrMo alloy in various simulated physiological solutions, Electrochim. Acta 78 (2012) 259–273.
[41] I. Milošev, CoCrMo alloy for biomedical applications, Biomedical Applications, Springer, 2012, 1–72.
[42] Y. Liu, J.L. Gilbert, Effect of simulated inflammatory conditions and potential on dissolution and surface oxide of CoCrMo alloy: In situ electrochemical atomic force microscopy study, Electrochim. Acta 262 (2018) 252–263.
[43] R. Namus, W. Rainforth, Influence of protein adsorption on tribocorrosion behaviour of CoCrMo biomedical-grade alloys, Tribol. Int. 150 (2020), 106364.
[44] J. Mystkowska, K. Niemirowicz-Laskowska, D. Łysik, G. Tokajuk, J.R. Dąbrowski, R. Bucki, The role of oral cavity biofilm on metallic biomaterial surface destruction–corrosion and friction aspects, Int. J. Mol. Sci. 19 (3) (2018) 743.
[45] A.E. Nel, L. Mädler, D. Velegol, T. Xia, E.M. Hoek, P. Somasundaran, F. Klaessig, V. Castranova, M. Thompson, Understanding biophysicochemical interactions at the nano–bio interface, Nat. Mater. 8 (7) (2009) 543–557.
[46] K. Gelderman, L. Lee, S. Donne, Flat-band potential of a semiconductor: using the Mott–Schottky equation, J. Chem. Educ. 84 (4) (2007) 685.
[47] Z. Zhang, J.T. Yates Jr., Band bending in semiconductors: chemical and physical consequences at surfaces and interfaces, Chem. Rev. 112 (10) (2012) 5520–5551.
[48] A. Fattah-Alhosseini, O. Imantalab, G. Ansari, The role of grain refinement and film formation potential on the electrochemical behavior of commercial pure titanium in Hank's physiological solution, Mater. Sci. Eng. C 71 (2017) 827–834.
[49] F. Fabregat-Santiago, G. Garcia-Belmonte, J. Bisquert, P. Bogdanoff, A. Zaban, Mott-Schottky analysis of nanoporous semiconductor electrodes in dielectric state deposited on SnO2 (F) conducting substrates, J. Electrochem. Soc. 150 (6) (2003), E293.
[50] I.M. Gadala, A. Alfantazi, A study of X100 pipeline steel passivation in mildly alkaline bicarbonate solutions using electrochemical impedance spectroscopy under potentiodynamic conditions and Mott–Schottky, Appl. Surf. Sci. 357 (2015) 356–368.
[51] E. Rahimi, R. Offoiach, K. Baert, H. Terryn, M. Lekka, L. Fedrizzi, Role of phosphate, calcium species and hydrogen peroxide on albumin protein adsorption on surface oxide of Ti6Al4V alloy, Materialia 15 (2021), 100988.
[52] O.R. Cámara, L.B. Avalle, F.Y. Oliva, Protein adsorption on titanium dioxide: effects on double layer and semiconductor space charge region studied by EIS, Electrochim. Acta 55 (15) (2010) 4519–4528.
[53] S. Karimi, A. Alfantazi, Electrochemical corrosion behavior of orthopedic biomaterials in presence of human serum albumin, J. Electrochem. Soc. 160 (6) (2013) C206–C214.
[54] S. Karimi, T. Nickchi, A. Alfantazi, Effects of bovine serum albumin on the corrosion behaviour of AISI 316L, Co–28Cr–6Mo, and Ti–6Al–4V alloys in phosphate buffered saline solutions, Corros. Sci. 53 (10) (2011) 3262–3272.
[55] S.S. Panda, H.E. Katz, J.D. Tovar, Solid-state electrical applications of protein and peptide based nanomaterials, Chem. Soc. Rev. 47 (10) (2018) 3640–3658.
[56] K. Rezwan, L.P. Meier, M. Rezwan, J. Vörös, M. Textor, L.J. Gauckler, Bovine serum albumin adsorption onto colloidal Al2O3 particles: a new model based on zeta potential and UV− Vis measurements, Langmuir 20 (23) (2004) 10055–10061.
[57] A. F-06, Standard Test Method for Conducting Cyclic Potentiodynamic Polarization Measurements to Determine the Corrosion Susceptibility of Small Implant Devices, ASTM International West Conshohocken, PA, 2001.
[58] Z. Esfahani, E. Rahimi, M. Sarvghad, A. Rafsanjani-Abbasi, A. Davoodi, Correlation between the histogram and power spectral density analysis of AFM and SKPFM images in an AA7023/AA5083 FSW joint, J. Alloy. Compd. 744 (2018) 174–181.
[59] E. Rahimi, A. Rafsanjani-Abbasi, A. Kiani-Rashid, H. Jafari, A. Davoodi, Morphology modification of electrodepositedsuperhydrophobic nickel coating for enhanced corrosion performance studied by AFM, SEM-EDS and electrochemical measurements, Colloid. Surf. A Physicochem. Eng. Asp. 547 (2018) 81–94.
[60] E. Rahimi, A. Kosari, S. Hosseinpour, A. Davoodi, H. Zandbergen, J.M.C. Mol, Characterization of the passive layer on ferrite and austenite phases of super duplex stainless steel, Appl. Surf. Sci. 496 (2019), 143634.
[61] B. Ter-Ovanessian, C. Alemany-Dumont, B. Normand, Electronic and transport properties of passive films grown on different Ni-Cr binary alloys in relation to the pitting susceptibility, Electrochim. Acta 133 (2014) 373–381.
[62] G. Ansari, A. Fattah-alhosseini, On the passive and semiconducting behavior of severely deformed pure titanium in Ringer's physiological solution at 37 °C: a trial of the point defect model, Mater. Sci. Eng. C 75 (2017) 64–71.
[63] Y. Long, D.G. Li, D.R. Chen, Influence of square wave anodization on the electronic properties and structures of the passive films on Ti in sulfuric acid solution, Appl. Surf. Sci. 425 (2017) 83–94.
[64] F.Y. Oliva, O.R. Cámara, L.B. Avalle, Adsorption of human serum albumin on electrochemical titanium dioxide electrodes: Protein–oxide surface interaction effects studied by electrochemical techniques, J. Electroanal. Chem. 633 (1) (2009) 19–34.
[65] N. Hakiki, M.D.C. Belo, A. Simoes, M. Ferreira, Semiconducting properties of passive films formed on stainless steels influence of the alloying elements, J. Electrochem. Soc. 145 (11) (1998) 3821–3829.
[66] J. Park, J. Yang, G. Lee, C.Y. Lee, S. Na, S.W. Lee, S. Haam, Y.-M. Huh, D.S. Yoon, K. Eom, Single-molecule recognition of biomolecular interaction via Kelvin probe force microscopy, ACS Nano 5 (9) (2011) 6981–6990.
[67] O. Cherniavskaya, L. Chen, V. Weng, L. Yuditsky, L.E. Brus, Quantitative noncontact electrostatic force imaging of nanocrystal polarizability, J. Phys. Chem. B 107 (7) (2003) 1525–1531.
[68] I. Spajic, E. Rahimi, M. Lekka, R. Offoiach, L. Fedrizzi, I. Milosev, Al2O3 and HfO2 atomic layers deposited in single and multilayer configurations on titanium and on stainless steel for biomedical applications, J. Electrochem. Soc. (2021).
[69] J. Lü, E. Delamarche, L. Eng, R. Bennewitz, E. Meyer, H.-J. Güntherodt, Kelvin probe force microscopy on surfaces: Investigation of the surface potential of self-assembled monolayers on gold, Langmuir 15 (23) (1999) 8184–8188.
[70] V. Palermo, M. Palma, P. Samorì, Electronic characterization of organic thin films by Kelvin probe force microscopy, Adv. Mater. 18 (2) (2006) 145–164.
[71] A. Imani, E. Asselin, Fluoride induced corrosion of Ti-45Nb in sulfuric acid solutions, Corros. Sci. 181 (2021), 109232.
[72] I. Milošev, H.-H. Strehblow, The composition of the surface passive film formed on CoCrMo alloy in simulated physiological solution, Electrochim. Acta 48 (19) (2003) 2767–2774.
[73] A. Hodgson, S. Kurz, S. Virtanen, V. Fervel, C.-O. Olsson, S. Mischler, Passive and transpassive behaviour of CoCrMo in simulated biological solutions, Electrochim. Acta 49 (13) (2004) 2167–2178.
[74] Y. Tanaka, K. Kurashima, H. Saito, A. Nagai, Y. Tsutsumi, H. Doi, N. Nomura, T. Hanawa, In vitro short-term platelet adhesion on various metals, J. Artif. Organs 12 (3) (2009) 182–186.
[75] L.N. Wang, A. Shinbine, J.L. Luo, Electrochemical behavior of CoCrMo implant in Ringer's solution, Surf. Interface Anal. 45 (9) (2013) 1323–1328.
[76] Y. Zhang, Y. Fung, H. Sun, D. Zhu, S. Yao, Study of protein adsorption on polymer coatings surface by combining quartz crystal microbalance with electrochemical impedance methods, Sens. Actuators B Chem. 108 (1) (2005) 933–942.
[77] D.D. Macdonald, The point defect model for the passive state, J. Electrochem. Soc. 139 (12) (1992) 3434.
[78] S. Karimi, T. Nickchi, A.M. Alfantazi, Long-term corrosion investigation of AISI 316L, Co–28Cr–6Mo, and Ti–6Al–4V alloys in simulated body solutions, Appl. Surf. Sci. 258 (16) (2012) 6087–6096.